Combining Additive Manufacturing and Biomimetics for the Optimization of Satellite Structures

D. Vogel[a]*, L. Geismayr[a], M. Langer[a], P. Leslabay[b], G. Schlick[c]

[a]*Institute of Astronautics, Technical University of Munich, Boltzmannstraße 15, 85748 Garching, Germany,* daniel.vogel@tum.de

[b]*Instituto Tecnológico de Buenos Aires (ITBA), Av. Eduardo Madero 399, Buenos Aires, Argentina,* leslabay@itba.edu.ar

[c]*Fraunhofer Research Institution for Casting, Composite and Processing Technology IGCV, Beim Glaspalast 5, 86153 Augsburg,* georg.schlick@igcv.fraunhofer.de

* Corresponding Author

Abstract

Successful utilization of Additive Manufacturing (AM) in the space sector implicates two aspects: First, an understanding of the process inherent characteristics has to be developed, where the anisotropic behavior of material is of significant importance. Second, the part design methodology has to be adapted, since it is often coupled and limited to traditional shapes and production methods and thus prevent an exploitation of the full AM potential. In a research collaboration between the Technical University of Munich, the Instituto Tecnológico de Buenos Aires, and the Fraunhofer Research Institution for Casting, Composite and Processing Technology, the structural optimization of a microsatellite yielded in research in both areas. In this paper the evaluation of the Total Mass Loss (TML), Coefficient of Thermal Expansion (CTE) and tensile strength for the materials polyether-ether-ketone (PEEK) and Ti6Al4V, which are both relevant for space applications, will be reported. Tensile and dilatometer specimen with orthogonal placement on the build platform for all three printing directions were produced via Fused Deposition Modelling (FDM) for PEEK and laser powder bed fusion (L-PBF) for Ti6Al4V in accordance to national standards. Outgassing tests of the specimen show that the TML for both materials is below the limit of 1%. CTE values deviate 13% from the manufacturers' specified mean value for injection molded PEEK. Mean tensile strength values for PEEK were 57% worse than the injection molded values specified by the manufacturer. Ti6Al4V samples showed no anisotropy and fitted the expected values for both, CTE and tensile strength. The overall results indicate the need for additional tests and safety factors when using additive manufactured PEEK for space applications. The second part of this paper presents a holistic design approach, composed of several already known methodologies. For the selection of suitable part candidates for AM specific redesign, different parts and assemblies in terms of manufacturability, economic feasibility and the potential of functional improvements were compared. For the subsequent part redesign, a biomimicry inspired design methodology in combination with AM design rules was applied, overcoming common thinking patterns. The approach was verified through a case study, where a star tracker's housing was systematically redesigned. The new design includes an integrated thermal link, which helps to keep the commercial off the shelf (COTS) sensor at low temperatures during operation, and an integrated compliant mechanism for the fine adjustment of the sensor. Finally, the design was validated through thermal analysis in ESATAN-TMS and structural analysis in ANSYS.

Keywords: Additive Manufacturing, PEEK, Ti6Al4V, Biomimetics, Materials & Processes, Satellite, Star Tracker

Acronyms/Abbreviations

AM	additive manufacturing
BFL	back focal length
COTS	commercial off the shelf
CTE	coefficient of thermal expansion
CVCM	collected volatile condensable material
ECSS	European Cooperation for Space Standardization
ESA	European Space Agency
FDM	fused deposition modelling
L-PBF	laser powder bed fusion
NASA	National Aeronautics and Space Administration
RML	recovered mass loss
TML	total mass loss
TRIZ	theory of inventive problem solving
TVAC	thermal vacuum

1. Introduction

Materials for space application are highly critical regarding their properties. By manufacturing the parts additively, the material's datasheets may not be applicable depending on the printing direction. This is caused by possible inhomogeneities of the part leading to disadvantages or weak spots in usage. Additionally,

any material used for space applications must sustain the unique environment in space. Determining the materials response to space-similar environment in a thermal vacuum (TVAC) chamber is necessary because the parameters given by the specific material's datasheets may vary, as standardisation is in the early stages of development and some data is missing. Chapter 2 thus describes the evaluation of PEEK and Ti6Al4V regarding outgassing, thermal expansion and mechanical properties.

To get the most out of AM, not only the material and process inherent characteristics must be considered, but also the part design approach, which is covered in chapter 3 of this paper. While novel parts can be designed completely from scratch to fit a certain application, the typical situation in the industry comprises of large catalogues of multiple parts, from which those parts must be selected and redesigned towards performance or functionality goals. Criteria are usually defined to support the selection of the most suitable candidates. A literature survey on part selection approaches shows that either few qualitative criteria or many quantitative criteria are proposed. A balanced approach is proposed, taking quantitative measures into account when information is available and focusing on qualitative characteristics when the precise properties of the parts are uncertain.

Most AM design methodologies focus on optimizing the shape or topology of a structure, but neglect further possibilities such as complexity of material, function and hierarchy. Since these principles and their combinations frequently occur in nature, a bioinspired part design can lead to unparalleled innovative solutions. Applying biomimicry to space applications may seem questionable at first sight, but equally extreme environments are present both in space and in nature. Supported by a design methodology developed by Fraunhofer [11], a star tracker housing was systematically redesigned with focus on implementing solutions inspired by biomimicry and AM's design freedom. Chapter 4 of this paper describes this design process, while chapter 5 shows a thermoelastic analysis of the resulting star tracker housing. The last chapter concludes with the implications of this work.

2. AM materials for space applications

The evaluated materials in this paper are PEEK and Ti6Al4V. Both materials are nowadays used for space applications as they show sufficient mechanical and thermal properties and can be handled by state of the art AM methods. But as these methods are relatively new, very few to no data is available describing material properties depending on printing direction. For example, AM is especially known for its inhomogeneities in z-axis, caused by its layered structure. Knowing these effects in advance is important for all design decisions later on. Therefore, tests were conducted to investigate the properties of AM PEEK and AM Ti6Al4V.

2.1. Sample production and geometry

PEEK samples used in this work were made of GEWOPEEK 260+ and were manufactured by FDM with a GEWO HTP260 machine. Printing layer thickness was 0,2 mm.

Ti6Al4V samples were made of EOS Titanium Ti64 and were manufactured with the L-PBF method on a EOSINT M270 Xtended machine.

After manufacturing, the samples were annealed under argon inert gas atmosphere at 800 °C for 4 h and later cooled down in the furnace. The aim of this process is the relief of stresses and thus get a more homogeneous material in all directions. This leads to a higher ultimate strain, but a reduction of tensile strength and yield strength [1]. The heat-treatment led to a slightly oxidized surface of the samples, most probably due to residual oxygen in the shielding gas atmosphere.. Therefore, it is expected to get different results of the properties compared to the received data sheet information.

After annealing, the samples were sandblasted to remove leftover supports of the production and the oxidised layer. By sandblasting the oxidised layer could be completely removed easily.

For the thermal expansion tests, both sample types, PEEK and Ti6Al4V, had the same dimensions: a length of 50,5 mm with a square base of 6 mm x 6 mm. DIN 51045 demands bevelled edges and even and plane parallel fronts [2], so the samples stand securely in the sample mount and do not manipulate the results by jiggling.

For the tensile tests, two different types of samples were needed as the standards for metal and plastics tensile samples varies: The Ti6Al4V samples were manufactured according to E 5x10x40 DIN 50125 [3], the PEEK samples match the ISO 527-2/1BA standard [4]. Because of problems in the manufacturing process, the XY samples were printed as a plate and later cut out conventionally. Fig. 1 shows the definition of printing directions, for all samples the building direction is in Z direction.

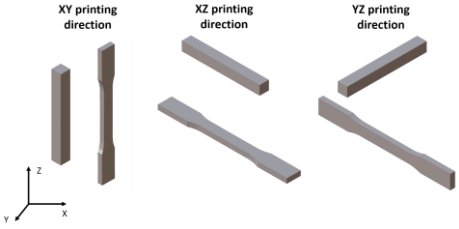

Fig. 1. Definition of directions for CTE and tensile samples, the Z axis is the building direction

2.2 Outgassing

TML of a material is important for flight acceptance as outgassing of substrates can harm the environment within a spacecraft, which could potentially alter the surrounding environment and harm other devices [5]. The ECSS-Q-ST-70-02C defines the acceptance criterion for space application with a mean value of <1 % TML, <1 % recovered mass loss (RML) and <0.1 % collected volatile condensable material (CVCM) [6], whereof the TML and CVCM are the most critical ones.

2.2.1 Test Setup

The performed test does not completely match the European Cooperation for Space Standardization (ECSS) standard [4] and only TML and RML were evaluated. The samples were pre-conditioned at 24,5 °C and 32 %rh for 24 h, the thermal vacuum test was done at 100 °C and $< 10^{-5}$ mbar for 24 h and post-conditioning at 23,1 °C and 24 %rh for 24 h. For both materials, PEEK and Ti6Al4V, four samples of each printing direction were tested, leading to a total of 48 samples.

2.2.2 Results

Average outgassing values for all printing directions are listed in Table 1. For all results the required standard error of mean value, given in the ECSS [7], of < 0,05 % was fulfilled.

Table 1. Average outgassing values for all printing directions and materials

	TML mean value [%]	RML mean value [%]
PEEK XY	0,17	0,08
PEEK XZ	0,14	0,08
PEEK YZ	0,13	0,07
Ti6Al4V XY	0,002	-0,001
Ti6Al4V XZ	0,003	0,001
Ti6Al4V YZ	0,002	0,001

All printing directions for PEEK showed very similar results. The difference for the XY printed PEEK for TML could be caused by the tensile samples as they were printed as a plate and manufactured conventionally. As a result, it is possible that impurities infiltrated the cutting edges and distorted the results. All other samples were directly manufacture by AM. The difference in TML and RML shows that about half of the outgassed material was water that was reabsorbed during post-processing.

Also, Ti6Al4V shows an independence of its printing direction. TML and RML values are beneath the accuracy of the used micro balance and therefore are practically not expressive. The negative RML for XY printed Ti6Al4V was caused by a measuring error or an impurity, like dust, making the sample slightly heavier. Metals typically show no outgassing. Nevertheless, they can release gases from cracks or impurities. As powder is the base material used for L-PBF, which offers a big surface, impurities could happen. Overall, no significant outgassing appeared. This means a very pure powder base material, without any impurities, was used for manufacturing. The difference in TML and RML shows that some of the outgassed material was water that was reabsorbed during post-processing.

2.3 Thermal Expansion

Thermal expansions can generate harmful internal stresses when a structural part is heated and either kept at a constant length or joint to another material with a different CTE. Because of the high temperature ranges in space applications the CTE of the AM manufactured materials is especially important to determine.

2.3.1 Test Setup

Samples were tested in a temperature range of -120 °C to +120 °C under helium atmosphere with a heating rate of 3 K/min and a bearing strength of 0,25 N.

Only XY and YZ directions were tested, as the geometry of the samples were the same for XZ and YZ direction. Each sample was tested at least two times to ensure that the measurement was not influenced by creeping and/or settling effects. For every material type and direction, two samples with and without exposure to TVAC environment were tested. For the XY printed Ti6Al4V, three samples were measured after TVAC exposure, as the first two samples did not align, which was different for every other sample group.

2.3.2 Results

Average CTE values for PEEK in all printing directions are shown in Fig. 2 and listed in Table 2.

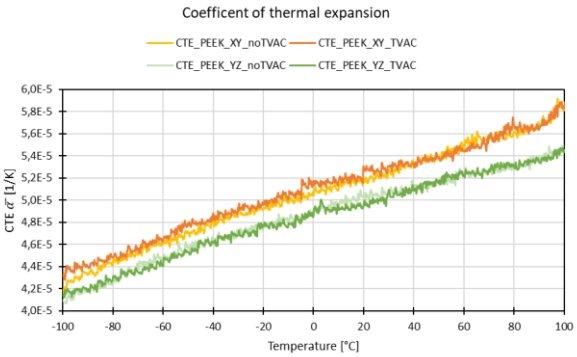

Fig. 2. Representative CTE curves for PEEK in all directions before and after TVAC exposure

Table 2. Average CTE values for PEEK in all printing directions

	Mean CTE $\alpha_{(-100,+100°C)}$ [10^{-6}*1/K]	True CTE $\alpha_{(-100° C)}$ [10^{-6}*1/K]	True CTE $\alpha_{(+100° C)}$ [10^{-6}*1/K]
PEEK XY – no TVAC	50,61 ±0,08	42,56 ±0,31	58,01 ±0,42
PEEK XY - TVAC	50,61 ±0,06	43,10 ±0,13	58,01 ±0,12
PEEK YZ – no TVAC	48,42 ±0,04	40,62 ±0,27	54,04 ±0,36
PEEK YZ - TVAC	48,21 ±0,01	41,43 ±0,19	54,28 ±0,08

Table 3. Average CTE values for Ti6Al4V in all printing directions

	Mean CTE $\alpha_{(-100,+100°C)}$ [10^{-6}*1/K]	True CTE $\alpha_{(-100° C)}$ [10^{-6}*1/K]	True CTE $\alpha_{(+100° C)}$ [10^{-6}*1/K]
Ti6Al4V XY – no TVAC	8,62 ±0,007	5,18 ±0,19	9,48 ±0,03
Ti6Al4V XY - TVAC	8,61±0,007	4,55 ±0,25	9,46 ±0,02
Ti6Al4V YZ – no TVAC	8,63 ±0,01	4,35 ±0,57	9,53 ±0,04
Ti6Al4V YZ - TVAC	8,61 ±0,006	5,31 ±0,33	9,42 ±0,01

It is recognizable, that the mean CTE for the same printing direction is nearly the same before and after exposure to TVAC environment for all AM PEEK samples. This is especially true for the mean CTE but also for the true CTE at +100 °C. At lower temperatures, values varied slightly more. It has to be noted though, that those samples not exposed to TVAC environment, hence were not heated up to 100 °C, show an increase of CTE in a temperature range of 60 °C to 80 °C. Samples that were already heated up at least one time do not show this behaviour. This effect can be seen in the diagrams in the appendix Fig. A1 and Fig. A2. The reason for this effect could not be completely determined, as the mechanical properties of PEEK show first weaknesses at 150 °C, but it can be said that annealing must be done to ensure constant material properties. Both printing directions show a linear increase of CTE, whereas YZ printed samples show a slightly superimposing with a logarithmic increase.

YZ values are beneath XY values. This can be caused by the layered manufacturing. Different layers may not be connected perfectly amongst themselves leading to defects with a higher expansion during thermal loads. In YZ printed material, whole connected strands expand which have a much better homogeneity.

Average mechanical values for Ti6Al4V in all printing directions are shown in Fig. 3 and listed in Table 3.

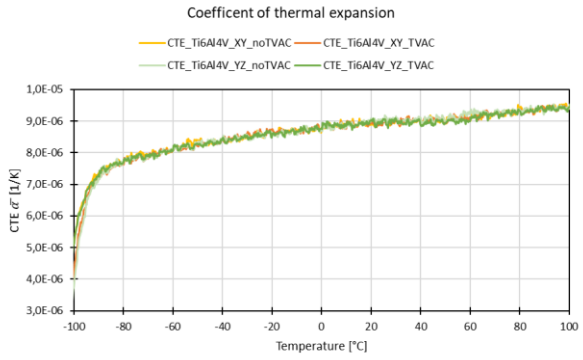

Fig. 3. Representative CTE curves for Ti6Al4V in all directions before and after TVAC exposure

Ti6Al4V samples all show a very consistent mean CTE independent of their printing direction and the environment they were exposed to. The independency of printing direction is most likely caused by the high manufacturing temperatures and annealing. This is also favoured by the powdery texture of the material, enabling a very fine structure. The independency of space conditions is also reasonable, as Ti6Al4V shows a maximum operating temperature of 350 °C and therefore no structural changes appear at temperatures of 100 °C. All samples show a logarithmic decrease. The measured values varied slightly more at lower temperatures up to -85 °C (see Fig. 3). The variation at lower temperatures can be caused by stresses at these temperatures. At higher temperatures these stresses, creeping or settling influences do not occur seemingly.

2.4 Tensile strength

The tensile test is aimed to determine the material's mechanical properties under tensile load. For space application materials have to withstand high loads, especially at the launch of a rocket.

2.4.1 Test Setup

Tests were conducted on a INSTRON 4505 universal testing machine. To conduct the measurements a 100 kN load cell was used for both materials. The used extensometer has a gauge length of 12,5 mm ±5 mm. For all Ti6Al4V samples the load was raised with a speed of 5 mm/min, for PEEK samples it was 1 mm/min. For every material type and direction four samples with and without exposure to TVAC environment were tested.

2.4.1 Results

Average mechanical values for PEEK in all printing directions are shown in Fig. 4 and listed in Table 4.

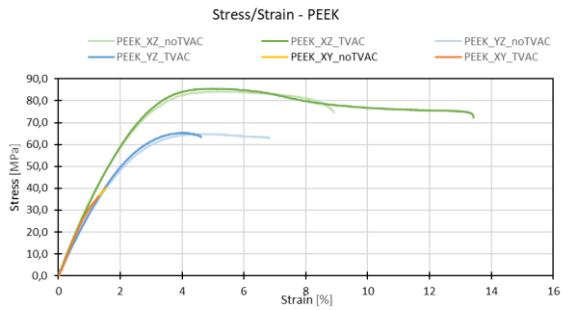

Fig. 4. Representative stress/strain curves for PEEK in all directions before and after TVAC exposure

Table 4. Average mechanical values for PEEK in all printing directions

	E-modulus E[GPa]	Tensile strength σ_m [MPa]	Breaking strength σ_b [MPa]	Total strain A_t [%]	Fracture strain A [%]
PEEK XY - no TVAC	3,36 ±0,12	41,08 ±2,18	40,95 ± 2,10	1,50 ±0,12	0,07 ±0,02
PEEK XY - TVAC	3,19 ±0,06	38,50 ±2,17	38,10 ±2,20	1,37 ±0,11	0,00 ±0,03
PEEK XZ - no TVAC	3,18 ±0,22	76,09 ±8,82	66,95 ±6,91	8,32 ±1,67	3,17 ±0,94
PEEK XZ - TVAC	3,22 ±0,08	87,25 ±0,98	75,86 ±2,37	12,69 ±0,95	4,94 ±0,76
PEEK YZ - no TVAC	3,22 ±0,17	63,51 ±1,29	61,19 ±1,37	5,20 ±0,68	1,29 ±0,26
PEEK YZ - TVAC	2,71 ±0,25	63,23 ±2,78	61,04 ±2,54	4,44 ±0,34	0,77 ±0,12

All printing directions show a different fracture mechanism. Overall values variate much more at higher stress levels, the lower levels fit together very nicely.

XY printed PEEK (with and without TVAC exposure) shows a brittle fracture, meaning that nearly no necking appears, and samples break straight after they reached their tensile strength. This results in a very low total strain and similar breaking strength compared to the tensile strength. The brittle fracture results in an even fracture surface, going exactly through one layer. This means the interconnections between the two layers broke. Generally speaking, materials exposed to TVAC showed slightly lower values compared to non-exposed ones.

XZ printed PEEK (with and without TVAC exposure) in contrast shows a though fracture, meaning recognizable necking appears, the total strain is very high and the sample breaks far after it reached its tensile strength. Similar to XY printed PEEK, strength variates more, but also total strain. The tough fracture results in a very constricted and uneven fracture surface. This is caused by the strands that run in a 45° angle to the applied force, leading to a much higher stability and resulting in better stress absorption and higher strain. Also, due to their 45° angle, strands can firstly slide before breaking completely. Opposite to the XY printed PEEK, TVAC exposed material shows higher strength and strain values that might be caused by homogenization of the samples in between the strands. The E-modulus remains the same as before.

YZ printed PEEK (with and without TVAC exposure) shows a combination of both fracture types, the brittle and tough fracture. Medium necking appears, and the total strain and strength values lie in between the XY and ZX printed values. Typical for the brittle fracture the samples broke shortly after they reached their tensile strength. Similar to XY printed PEEK, strength values vary more than the E-modulus or the strain values. The mixture of the structure types results in a medium constricted but relatively even fracture surface. The fracture occurs not exactly through one certain layer but is more even than for XZ printed samples. This is caused by the strands that run parallel to the applied force, which have a much higher stability, resulting in better stress absorption and higher strain. As the sample was not completely filled with material, the YZ samples were of limited quality (air-gaps) and thus strands were not likely to slide, resulting in values lower than for XZ printed material. TVAC exposed material shows similar strength and strain values, which might be again caused by homogenization of the samples in between the strands.

Average mechanical values for Ti6Al4V in all printing directions are listed in Table 5.

Table 5. Average mechanical values for Ti6Al4V in all printing directions

	E-modulus E [GPa]	Tensile strength σ_m [MPa]	Breaking strength σ_b [MPa]	Total strain A_t [%]	Fracture strain A [%]
Ti6Al4V XY – no TVAC	109,41 ±2,34	1000,72 ±0,60	963,62 ±7,60	4,44 ±0,08	2,01 ±0,08
Ti6Al4V XY – TVAC	113,72 ±2,28	1008,11 ±2,70	969,76 ±1,77	4,48 ±0,06	1,96 ±0,05
Ti6Al4V XZ – no TVAC	113,48 ±2,10	1005,47 ±3,54	980,52 ±2,89	4,84 ±0,08	2,50 ±0,09
Ti6Al4V XZ – TVAC	112,18 ±1,86	1007,94 ±1,15	987,97 ±4,19	5,00 ±0,24	2,61 ±0,19
Ti6Al4V YZ – no TVAC	112,65 ±1,41	1020,56 ±1,16	1003,07 ±2,39	5,11 ±0,11	2,58 ±0,09
Ti6Al4V YZ – TVAC	108,43 ±2,67	1022,02 ±3,62	1003,08 ±3,66	4,88 ±0,19	2,51 ±0,11

It is recognizable, that all printing directions of Ti6Al4V show very consistent values for E-modulus, independent of their printing direction or the

environment they were exposed to. As before, the independency of printing direction is most likely caused by the high manufacturing temperatures.

XY printed samples show the lowest strengths and strains, meaning they show the most brittle fracture. Also, minimum necking appears compared to the other samples. This is most likely caused by the layer wise building up and therefore worse interconnections between two layers. This does not affect the values as much as it did for PEEK, and unlike PEEK the fracture surface is not even or going exactly through one layer. All printed directions show a variation of the three appearing fracture types:

- 0° fracture surface in the middle and a 45° shear fraction that starts after the microvoid's cavity reached an edge (initiating point)
- cup & cone fraction
- mixture between the two of them

XZ values showed medium values compared to the other printing directions with the same strain values as YZ printed samples. YZ values showed the highest strength values and same strain values as XZ printed samples.

3. Systematic selection of suitable parts

Literature review showed that three opposite methodologies are proposed to select suitable parts for AM specific redesign. Klahn [8] proposes four qualitative criteria, which allow for a quick evaluation of larger numbers of parts. Stacheder [9] summarizes various proposals of AM checklists, which are utilized to determine whether the part candidate has design features that would favor AM as the manufacturing process. This qualitative evaluation is then extended by a quantitative rating comparing the parts geometrical features to the capabilities of the selected AM process. At the center of the methodology proposed by Lindemann [10] stands an extensive trade-off matrix, which allows for a detailed evaluation of a part. The candidates are evaluated through a value benefit analysis based on various categories and criteria, resulting in a quantitative distinction of the parts.

The selection approach in this paper is based on the trade-off matrix published by Lindemann [10], which is shortened and adapted to the present situation. A weighted point rating is preferred over the originally proposed value benefit analysis, because it is simpler in implementation. Furthermore, the value benefit analysis performs best in situations where many parts must be evaluated and ranked using quantitative selection criteria. Such ranking is not necessary in the present work since only the best alternative will be chosen for a redesign. The definition, rating and weighting of the here presented criteria was discussed with both experts from the AM sector and the space sector.

These criteria are divided into the four classes that represent relevant aspects of the present use case: Manufacturability, Material, Economics and Design & Functionality. It is important to mention that this list of criteria must be adapted to the specific part portfolio and use case. For example, if the portfolio contains parts of vastly varying order of magnitude or quantity, it is necessary to formulate additional criteria regarding these subjects.

3.1 Manufacturing Criterion

The following two criteria help to identify parts, which are suitable for AM from a manufacturing point of view:

- Does the design space of the part or assembly fit into one of the available build chambers?
- Does the part require features that are difficult to manufacture via AM?

At first it is verified, whether the part or assembly would fit into the build volume of one of the available AM machines. The exact dimensions of the later to be manufactured part are often unknown at the selection stage. Nevertheless, basic engineering information such as available design space is usually known and allows for a preliminary estimation of the manufacturing feasibility.

Subsequently it can be verified whether the part requires design features that are difficult or impossible to manufacture via AM. Different AM processes have different capabilities and restrictions, which is why it may be necessary to exclude certain processes at this early stage of development. For example, if a part requires large solid block structures, then L-PBF might be not the optimal choice, because thermally induced residual stresses are likely to occur during production.

3.2 Material Criterion

The material criterion helps to ensure that only a part with material requirements that can be fulfilled by a commercially available AM material is chosen. Relevant material properties can be, for example, electrical conductivity, magnetism or strength.

- Does an available AM material fulfill material-specific requirements?

3.3 Economical Criterion

The following criteria aim to include economic aspects in the part selection process. They do not represent a holistic evaluation, because it would require detailed information about the costs accumulated during the manufacturing of the original parts. Due to the absence of this information for the presented case, the great variety of cost estimation models that are available in literature is reduced to two criteria:

- Is the part complex to manufacture (high buy-to-fly ratio)?

- Is the part critical for the entire product development process or subject to late design changes?

The buy-to-fly ratio (mass of final part divided by feedstock material) is a dimension that gives the engineer an idea of how much waste material is generated during the manufacture of a part. A high ratio indicates the generation of a lot of waste material, which can correspond to increased cost. Some AM processes such as L-PBF allow for partial reuse of the feedstock and thus reduce cost. However, it must be kept in mind that the by-to-fly ratio is a very coarse measure to evaluate a part, since it does not cover the costs for AM-specific preparation and post-processing steps. Additionally, the costs of powder material for AM and solid feedstock for traditional manufacturing can differ significantly.

AM can facilitate a great reduction of lead time and is thus suitable for parts that are critical in the development process (e.g. necessary for testing other components) or for parts that are likely to be subject to late design changes. Therefore, the use of AM can lead to economic advantages of the single part, as well as to the reduction of the overall project cost.

3.4 Design and Functionality Criterion

The following three criteria aim to project possible improvements of the design and the functionality of the part through the increased freedom of design granted by AM:

- Is there lightweight potential through design for AM or topology optimization?
- Is it possible to merge adjacent parts, which are originally not manufactured in one piece because of manufacturing constraints?
- Is it possible to merge adjacent parts, which are fulfilling separate functions or add functionality through novel features?

With AM, the designer can utilize lattice structures or optimization techniques to create a part with vastly reduced weight. While these structures or the resulting topologies are unfeasible for manufacturing through traditional processes, they can be produced easily via AM.

An assembly consisting of multiple parts is more prone to failure than an assembly consisting of fewer parts, because more joints with failure potential must be utilized. This is especially true for assemblies that require high precision, e.g. optical components. AM opens the possibility to manufacture more integrated designs, so that the number of parts within an assembly can be reduced by merging adjacent parts into one.

In addition to above statements it can also be possible to improve the performance of a part or even add desirable functionality through novel features. The criterion used here aims to reflect the potential for innovative solutions which are possible by utilizing AM as manufacturing method.

4. Design of a star tracker housing

Using the previously described criteria, a star tracker housing was selected from a pool of four microsatellite parts (star tracker housing, resistojet support structure, primary structure and mounting bracket) for an AM specific redesign.

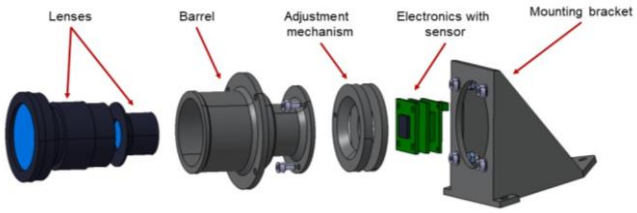

Fig. 5. Original star tracker without baffle

A star tracker typically consists of a barrel containing refractive optics (lens system), which focus light onto a sensor. The sensor, which is a commercial off the shelf (COTS) part in the present case, is usually adjustable through a mechanism to ensure that the active sensor surface is located within the back focal length (BFL) of the optics. A baffle reduces the amount of straylight entering the barrel, which is mounted onto the spacecraft structure with a bracket. The star tracker that was provided for this work is displayed in Fig. 5.

The star tracker fits well into typical build volumes of AM machines and does not require any features that are difficult to achieve via AM. Manufacturing and assembling of star trackers are often complex and reducing the number of components does not only have economic advantages but reduces risk as well. Nevertheless, requirements and the demanding space environment create opportunities for novel solutions that are only feasible using AM as means of production.

4.1 Biomimicry-based approach

The design process proposed by [11] utilizes the general methodological framework of the Theory of Inventive Problem Solving (TRIZ) to make the vast solution space offered by bionics accessible. Fig. 6 summarizes the TRIZ-based biomimetic part design process in form of a flowchart. The following subsections showcase this approach by the example of the star tracker housing.

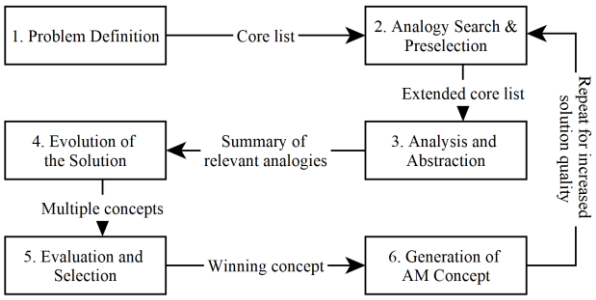

Fig. 6. Flowchart of the biomimicry-inspired methodology proposed by [11], the single steps are described in the following subsections

4.1.1 Problem definition

The main goal of the problem definition is to document the actual state of the part, including all functions it fulfills, as well as its components, connections and environmental/ boundary conditions. Analyzing the interaction between these elements yields a functional model (see Fig. A3) from which the core list is extracted. This list contains all relevant subfunctions of the star tracker on a very basic and abstract level. Some subfunctions are derived from the functional modelling by identifying negative effects that shall be minimized to improve the system, other subfunctions result from given requirements (see Table 6).

Table 6. Core list of the star tracker with priorization (1=highest priority)

Priority	Subfunction	Source
1	Maintain dimensional stability (thermo-structural)	Main function
2	Maintain dimensional stability (structural)	Main function
1	Enable adjustment of sensor	Requirement
2	Dissipate heat from sensor	Negative effect
3	Mitigate shock loads	Negative effect

The most ubiquitous environmental influence on the star tracker's performance are temperature related effects. On one hand, temperature gradient within the star tracker can lead to thermal deformations, which impair the alignment of optical elements, e.g. lenses and sensor, resulting in bad accuracy. On the other hand, uniform variations of the bulk temperature cause a change of the BFL and the lenses glass refraction index, and can even lead to additional noise or processing issues [12-14]. Additionally, the COTS sensor of the present star tracker is required to be kept at temperatures around – 10 °C during operation.

The dimensional stability of the optics is also endangered by structural loads during launch, where the supporting structure of the star tracker is required to have enough rigidity and strength.

Shock loads induced onto the star tracker during launch can impair the alignment of the optical components or even damage them, especially if internal stresses are present. Vibrations on orbit, caused by flywheels or jitter from attitude control thrusters, can lead to additional issues if they match a natural frequency of the star tracker [13].

The subfunctions presented here thus cover the most fundamental aspects that must be considered during the design of a star tracker. Other aspects that were neglected in this initial study include stray light, which requires an adequate baffle design, and high energy radiation, which can lead to noise and processing issues of the focal plane and lens degradation. [14]

4.1.2 Analogy search & preselection

Because the subfunctions of the star tracker are formulated on an abstract level, they can be solved by transferring solutions from the field of biomimicry. The source for the analogy search are biomimicry databases such as "AskNature" (www.asknature.org), because they are more accessible than consultation of scientific publications in the field of biology or interviews with biologists. The key challenges are identifying similarities and differences between analogies and subfunctions, screening relevant information and reducing the vast solution space to few but convincing phenomena.

It is important to mention that in this work, the search for possible solutions is not limited to biological analogies. Technical solutions that are tried and tested in the space sector and non-biological concepts are also included when improvements through the utilization of AM are expected.

4.1.3 Analysis and abstraction

Once fitting biological phenomena have been found, they must be completely understood (analysis) and reduced to their core principle (abstraction) before they can be transferred to the technical problem. This is a crucial and often underestimated step, because most phenomena have a variety of hidden influencing factors. While analyzing the analogies, one must especially focus on characteristics that can be influenced by AM, e.g. external and internal structure, material, surface and hierarchy. Possible biological and technical solutions for the subfunctions of the star tracker are listed in the following. A concise description of each solution as well as related literature is given in [15].

Maintain dimensional stability (thermo-structural):

- Integrated insulation
- Phase change material
- Low thermal expansion material

- Low/ zero thermal expansion lattice

Maintain dimensional stability (structural):

- Nature-inspired structures
- Turtle-inspired vault structuring
- Topology optimization

Enable adjustment of sensor:

- Compliant mechanism
- Traditional mechanism

Dissipate heat from sensor:

- Integrated thermal link
- Integrated heat pipe
- Increased radiator surface
- Compliant mechanism louver

Mitigate shock loads:

- Particle damper
- Auxetic lattice structures
- Woodpecker inspired shock absorber

4.1.4 Evolution of the solution

During this step, comprehensive solutions are generated from the single solutions of the respective subfunctions. To create this overall solution, different combinations of solutions fulfilling different subfunctions are compared with regards to contradicting requirements in a morphological box. With the help of this box, three concepts were developed during a workshop with participants from both the satellite technology and AM sector.

- Concept 1: Simple and cost-effective solutions
- Concept 2: Focus on bioinspired solutions
- Concept 3: High performance solutions

Table 7. Solutions for the subfunctions (concept 1)

Subfunction	Solution
Maintain dimensional stability (thermo-structural)	Integrated insulation
Maintain dimensional stability (structural)	Topology optimization
Enable adjustment of sensor	Compliant mechanism
Dissipate heat from sensor	Integrated thermal link + increased radiator surface
Mitigate shock loads	Particle damper

The first concept is selected for further development because it is expected to achieve sufficient performance improvements compared to the original star tracker. In addition, it is rated to be the most feasible concept in terms of technical implementation at current state of the art. Concepts 2 and 3 are not part of this paper but can be found in [15]. In the following, the solutions of concept 1, also shown in Table 7, are explained in detail:

Topology optimization is commonly utilized in combination with AM, because the resulting geometries are often difficult or impossible to produce through traditional processes, but easily manufacturable with AM. Using this approach, a significant amount of mass can be saved while the part's rigidity and stiffness is barely affected. It is also possible to add constraints that maximize the eigenfrequencies of the part, making it less prone to vibration excitations.

Compliant mechanisms are monolithic structures that can achieve motion, force, or displacement through the elastic deflection of flexible members. They bear the potential to improve the performance of space mechanisms in many aspects, which are extensively described in literature [16]. The most relevant advantages for the adjustment of the star sensor are:

- Elimination of backlash
- Predictability of hysteresis
- Reduced risk of joint misalignment (less assembly steps required)
- Reduced thermal gradient within the mechanism

Despite their advantages, compliant mechanisms also bear more challenges when compared to conventional mechanisms, especially if AM is considered for manufacture as described by [16, 17].

A straightforward approach to cool the sensor to the required operating temperature is to increase the heat dissipation by connecting the sensor to a heat sink. The thermal link could be integrated into the structure of the star tracker as to reduce the amount of necessary assembly steps. However, the thermal link must be insulated from the remaining star tracker structure to reduce heat losses along the link. This can be achieved using integrated insulation lattices as displayed in Fig.7. Since the heat conducting cross section of these lattices is significantly smaller than solid material, the effective thermal conduction can be reduced.

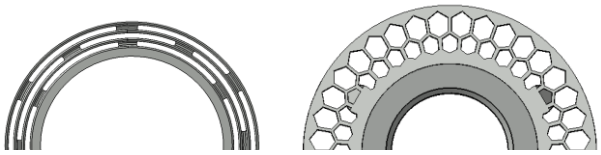

Fig. 7. Exemplary integrated layered insulation (left) and honeycomb lattice (right) to limit heat flow in radial direction

Particle damper are passive vibration damping devices which comprise of cavities that are filled with particles moving freely and producing an attenuation effect as they collide with one another and the walls of the cavity. Their advantages – easy implementation, excellent performance under a wide range of vibrational spectrums, and varying thermal environments – make them suitable for many space-related applications [18, 19]. AM is expected to further increase the potential of particle dampers, since the device can be integrated at

the optimal location of the structure. Furthermore, the geometry of the cavity can be optimized and still be manufacturable with AM.

4.1.5 Evaluation and selection

The evaluation and selection of the concepts is a two-step process: At first, all three concepts are compared to the original star tracker with regards to their performance and fulfilment of the core list. Subsequently, the three concepts are compared against each other using several criteria, e.g. development expenditure and required process chain, to determine the feasibility of their technical implementation. The first concept received the highest score in a weighted point rating and is preferred over concept 2 and 3 as described in subsection 4.1.4.

4.2 Generation of AM suitable concept

Fig. 8 shows the redesigned integral star tracker housing featuring a thermal link, which is insulated from the barrel by means of a honeycomb structure. Research regarding an integrated compliant mechanism for the adjustment of the sensor with one translational and two rotational degrees of freedom is not yet completed and thus omitted in this paper. Note that the particle dampers are not implemented in the detailed design of this case study to reduce the complexity of the development.

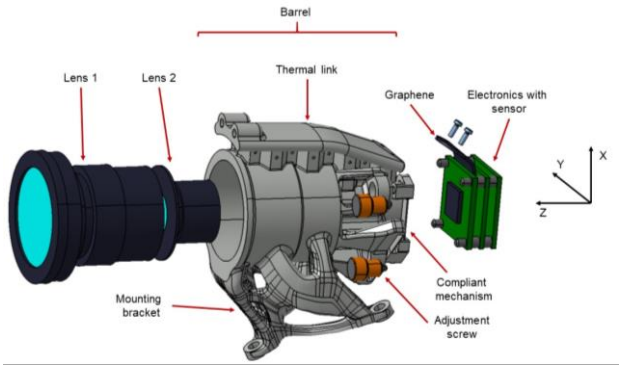

Fig. 8. CAD model overview of the redesigned star tracker housing, Z axis is equivalent to the optical axis

The following subsections explain the selection of the AM process and material, as well as the thermal and structural design.

4.2.1 Choice of process & material

Metal based L-PFB is selected as manufacturing process for various reasons. First, L-PBF allows for an unrestricted analysis of different types of satellite parts, because this process is compatible with a wide range of materials (e.g. polymers, metals and ceramics) [20]. In addition to that, L-PBF provides better tolerances and allows for more complexity than powder- or wire-feed AM, although it has a lower build rate [21]. This characteristic matches with the requirements for parts of the space sector, which usually employs low-volume, high-complex parts [20]. Also, L-PBF is increasingly used for final part production in the industry [20], which indicates that this process group is suitable from both technical and economic perspectives. Finally, most of the available AM machines at the Technical University Munich utilize the L-PBF process. In-house manufacturing of a technology demonstrator is both quicker and cheaper than making use of industrial services.

Three materials are available at the L-PBF machines of the Technical University Munich: Ti6Al4V, AlSi10Mg and AlMgSc (tradename Scalmalloy). Despite having very good mechanical properties, Ti6Al4V is ruled out due to its low thermal conductivity, which makes cooling of the sensor via a solid thermal link unfeasible (see 4.2.2). Scalmalloy is the preferred material, because it combines good mechanical properties with good thermal conductivity. However, the minimal wall thickness of this material is larger than the required thickness of the honeycomb cells, which is why it cannot be used. The remaining alloy, AlSi10Mg, has both the required thermal conductivity and the manufacturing capabilities that are required and is therefore chosen for the star tracker housing.

4.2.2 Thermal design

Fig. 9 displays the general thermal concept that is developed for the star tracker. The sensor is connected to a thermal link, which transfers the generated heat to a radiator where it is dissipated into space. The thermal link is insulated from the barrel to prevent heat losses and nonuniform distortions of the barrel, which could impair the alignment of the lenses. For the same reason, an insulating layer is attached on the interface between sensor and adjustment mechanism. The star tracker is insulated from the satellite to reduce its sensitivity to temperature changes of the spacecraft. This design is common among star tracker [12, 22, 23]. The baffle is physically separated from the star tracker, which eliminates any conduction between these parts. Another suitable concept for future work would be to connect the thermal link to the baffle, which eliminates the need for an additional radiator.

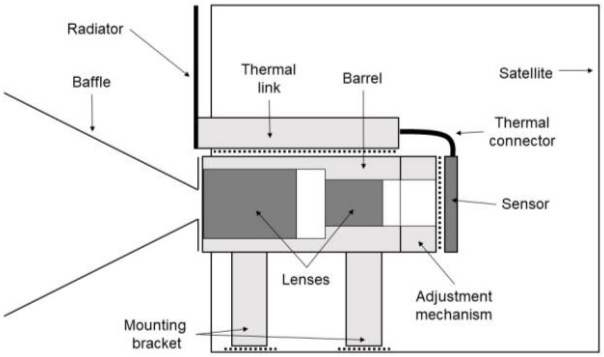

Fig. 9. Thermal concept of the star tracker, dotted lines represent insulation

ESATAN-TMS 2017 sp2 was utilized to generate a simplified thermal model for the initial sizing of the components (see Fig. 10). A detailed thermal model was derived from CAD at a later stage of the development, when precise information about the geometry was available.

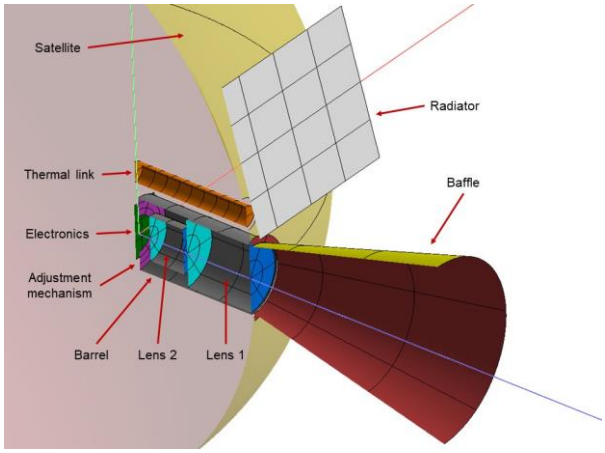

Fig. 10. Simplified thermal model in ESATAN-TMS

All components were modeled through shell element, except the thermal link, which was modeled through solid elements. The lenses, which are preassembled components of unknown internal setup, were modelled by two disks that are connected by a cylindric aluminum encasement. The satellite on which the star tracker is mounted, was modeled as sphere with a constant temperature of 10 °C. Small parts, for example wires or bolts, were not modeled as shells or solids, because their contribution to the total radiative heat transfer is negligible [23]. Instead, they were modeled as simple conductive links.

Whenever available, end-of-life values were utilized for the optical properties of the various materials to maintain a conservative simulation. The values for the transmissivity of the lens material BK-7 was selected by worst-case assumptions: Low transmissivities in the infrared-range lead to an increase of the sensor temperature, because the generated heat cannot be well radiated into space. High transmissivities in the ultraviolet-range cause the sensor to heat up quicker when it is directly exposed to the sun.

As mentioned before, the thermal link must be insulated from the barrel. This was realized through a honeycomb core structure, which has a significantly lower effective conductivity than solid material. Gilmore [22] presents a formula with which the effective thermal conduction can be calculated. The dimensions of the honeycomb structure were iteratively varied in accordance to the available design space and material capabilities (minimal wall thickness), until a sufficiently low effective thermal conductance of 7,5 W/(m²K) was reached.

Since no mission-specific orbit was defined in the requirements, an arbitrary solar synchronous orbit was selected (see Table 8). Star tracker are usually pointed away from the sun, which is why the primary pointing (optical axis/ Z axis) was defined to coincide with ESATAN's ANTI_TRUE_SUN vector. Thus, the optical axis is always oriented opposite to the sun vector. The secondary pointing ensures that the heat flux from earth and albedo onto the radiator is minimal.

Table 8. ESATAN-TMS orbit parameters for the nominal case

Parameter	Value
Eccentrity	0
Semi-Major Axis	6971 km
Altitude of Apogee	600 km
Altitude of Perigee	600 km
Inclination	97,8°
Right Ascension	30°
Argument of Periapsis	0°
Primary pointing (Z axis)	ANTI_TRUE_SUN
Secondary pointing (Y axis)	ZENITH
Omega (rotation about X axis)	0°

The robustness of the thermal design is verified by conducting analyzes with two hot cases. These hot cases consist of an initial nominal case orbit, followed by an event orbit during which the primary pointing vector of the star tracker is varied over time (see Table 9)

Table 9. Time dependent pointing properties for the event orbits A and B

Time [s]	Omega A [°]	Omega B [°]
0	0	0
300	170	90
360	170	90
660	0	90

During hot case A, the star tracker is rotated 170° about its X axis within five minutes, which almost points the optical axis directly into the sun. This position is kept for one minute before the star tracker rotates back into the initial orientation within five minutes. During hot case B, the star tracker is rotated 90° about its X axis within the same time intervals. These cases represent artificial scenarios, where intentional or unintentional deviations of the satellite pointing lead to additional heat loads onto the star tracker. Another ten nominal orbits are pursued after the event orbit to analyze how fast the star tracker recovers from these events. Additionally, a cold case orbit is simulated to verify that the sensor temperature stays above its minimal limit when it is switched off and does not generate heat.

The results for the sensor temperature obtained in the detailed model are displayed in Fig. 11. Although the initial, simplified thermal model indicated that a sensor temperature of approximately -10 °C is possible, analysis with the detailed thermal model yields an orbital temperature oscillating around +1 °C during a nominal case orbit. It is assumed that the target temperature of -10 °C can be achieved by improving the insulation between the sensor and the star tracker housing. The analysis also shows that the hot case events only have a marginal influence on the sensor temperature, resulting in temperature spikes not higher than + 5°C. The lower bound survival temperature (- 30 °C) of the COTS sensor is not reached during the cold case event. Although these results were obtained with a detailed model, an uncertainty of ± 20 °C is suggested, since a correlation with experimental values has not yet been conducted.

The maximal temperature gradient within the components of the star tracker as well as the fluctuation of the average temperature during one orbit are displayed in Table B2. Both dimensions are low for all components within the star tracker. This confirms the previous claim that the thermal conductance within the parts is sufficiently high and the general thermal concept is robust against hot case events.

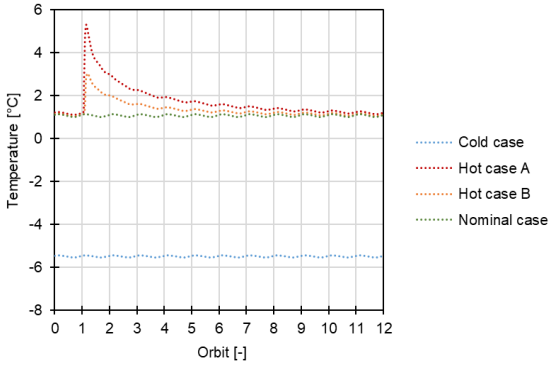

Fig. 11. Sensor temperature, the spikes of hot case A and B result from the event taking place at the beginning of the second orbit

4.2.3 Structural design

The software "solidThinking Inspire 2017.1" contains a topology optimization module using the "Optistruct" solver and is an easy-to-use software geared towards the designer rather than the FEM specialist. It is utilized to explore a possible design concept for the mounting bracket, although an optimization with a thermal objective function or constraint, e.g. minimization temperature gradients, is not possible.

The star tracker is mounted with three grounded bolts, which constrain the displacement of the bore holes in the non-design space. The acceleration loads with a value of 15g are applied to the geometry to comply with the required 12g acceleration including a sufficient margin. The optimization is conducted for six load cases, which cover both signs of the three orthogonal spatial directions (+X, -X, +Y, -Y, +Z and -Z).

Fig. 12. Topology optimization design space (left), raw result (center) and post-processed result (right)

Since dimensional stability is the main concern for the star tracker, the objective of the optimization is set to maximize the stiffness subject to the following constraints:

- Target volume: 20% of design space
- Maximize frequencies
- Minimum member thickness: 4 mm

The target volume constraint is used to specify the amount of material to keep within the design space. By setting a maximize frequency constraint, the solver will take eigenfrequencies into account and increase them as much as possible. The minimum member thickness

constraint ensures that the result does not include features with a cross section diameters smaller than the specified 4 mm. The topology optimized and integrated mounting bracket is 36% lighter than the original part.

5. Thermoelastic analysis of the star tracker housing

The thermoelastic behavior of the star tracker is analyzed with the finite element method. In this work, ANSYS 17.1 workbench and mechanical are utilized to carry out the analysis. The primary goal of the static thermal analysis is to quantify the displacement of the sensor with respect to the BFL while being subjected to the varying thermal environment on orbit. Furthermore, stresses caused by constraint thermal expansion are extracted. For this purpose, a point cloud containing the nodal temperature data from the detailed thermal model is exported from ESATAN-TMS and mapped on the finite element model. The following two cases are analyzed for reasons stated below:

- Nominal case: Verify that sensor displacement and thermal stresses are within the tolerance limits during nominal operation
- Hot case A: Verify that the sensor displacement and thermal stresses are within the tolerance limits during a hot case event or quantify the time necessary to return to operating conditions if these limits are exceeded

5.1 Setup

The point-cloud extracted from ESATAN-TMS contains the coordinates and the time-dependent temperature of each node. Each timestep of the thermal analysis corresponds to one load case in the thermoelastic analysis. However, the large number of available timesteps of the thermal analysis exceeds the computational limit of the workstation, which is why only ten timesteps are selected. Every 10^{th} timestep of the nominal case is utilized to analyze the star tracker's thermoelastic behaviour during one orbit. The nodal temperatures of the star tracker vary only marginally during the nominal case orbit and utilizing every 10^{th} timestep, which corresponds with time intervals of 10 minutes, models the thermal behaviour with sufficient precision. For the hot case, the timesteps of maximal sensor temperature of the event orbit and the nine subsequent nominal orbits are utilized instead of periodic time intervals. This allows to directly draw conclusions about the operability of the star tracker, since the sensor's compliance with both the temperature and displacement limit are known for these load steps.

The mapping of the temperatures is conducted separately for the barrel and lens system plus sensor to prevent mismatches (see Fig. 13). 109 source nodes are mapped onto 122448 target nodes of the barrel and 81 source nodes are mapped onto 10938 target nodes of the lenses and sensor.

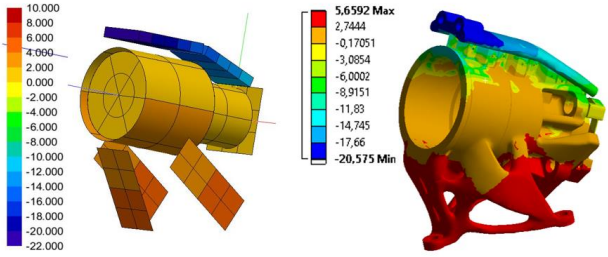

Fig. 13. Nominal case temperature field of the detailed thermal model (left) mapped onto barrel (right)

5.2 Sensor displacement

To precisely measure the deviation of the sensor with respect to the BFL plane, not only the thermal displacement of the sensor must be considered, but also the thermal displacement of the BFL plane. The latter is dependent on the thermal expansion behaviour of the lens system. Since the internal structure, and thus the internal thermal displacement, of the COTS lenses was unknown, the rear surface of lens 2 is selected as reference. Deviations in Z direction can move the sensor out of focus, which is why they must be limited at all means. Deviations in X and Y direction are not as critical and thus not presented in this paper.

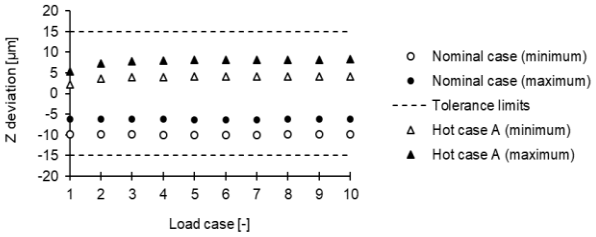

Fig. 14. Deviations of the sensor surface with respect to the BFL plane in Z direction)

Fig. 14 shows that the displacement of the sensor surface with respect to the BFL plane is within the required ± 15 µm tolerance limit for both nominal and hot case A. However, the hot case deviation does not return to the nominal case values within the analyzed nine subsequent orbits after the hot case event. Multiple consecutive hot case events could elevate the displacement beyond the limits, because of this long time that is necessary to recover. The angular displacement (see Fig. 15) exceeds the limit of 20 arcsec by far but fluctuates only approximately 0,7 arcsec around the average during a nominal case orbit. Thus, the angular deviation can be encountered by adjusting the sensor in the opposite direction before launch.

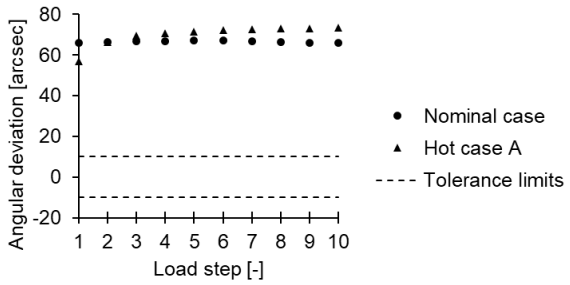

Fig. 15. Angular deviation of sensor surface with respect to the BFL plane

5.3 Thermal stresses

Tables B3 and B4 display the maximal equivalent thermal stresses occurring at the respective time steps of the nominal and hot case. In both cases, the resulting maximal stresses are located within the barrel and well below the yield strength of AlSi10Mg, eliminating concerns of structural failure due to thermal stresses.

6. Conclusion

6.1 AM materials for space applications

Outgassing: Both materials show values far beneath the National Aeronautics and Space Administration (NASA) and European Space Agency (ESA) requirement of <1 % and therefore can be used for space applications without any concerns.

Thermal expansion:

PEEK can be used for space applications. It shows low dependencies on printing directions. The one thing that has to be kept in mind is to heat the material above 100 °C beforehand, if temperatures above 60 °C are expected, in order to prevent defects caused by the first-time higher expansion between 60 °C and 80 °C.

Ti6Al4V shows isotropic behaviour and can be used for space applications without any concerns. The fast increase of the CTE value at temperatures up to -80 °C has to be considered, but this effect is only noteworthy for deep temperature applications.

Tensile strength:

PEEK can be used for space applications, but it has to be noted, that the printing direction makes a huge difference for mechanical properties.

Comparing the results for Ti6Al4V to the expected datasheet values [1] shows, that our results fit very well except for the strain values. This is most likely caused by an error in the annealing process, described in section 2.1.2, leading to a very brittle structure and therefore lower strains. It is not certain what happened during annealing and metallographic analysis is not yet finished. Nevertheless, the material can be used for space applications without any concerns. Most values are perfectly in accordance with the data sheet values.

6.2 Part selection & redesign

The results of the part selection match well with the unbiased intuition of experts in additive manufacturing, which is why the presented criteria are considered valid for the evaluation of parts for the redesign. Thus, the presented list is expected to perform well when a small number of parts must be evaluated.

Although many biological analogies were identified only few made it into the final concepts of the star tracker. The large number of subfunctions resulting from the complexity of the part increased the expenditure of the solution search. The authors were facing a multitude of possible analogies for the various subfunctions, but it was not possible to achieve the comprehensive understanding for all of them which would be necessary to find the best fitting solution.

Nature-inspired cellular structures with gradually changing properties (e.g. cell width or thickness) bear an unparalleled potential. Not only do they facilitate designs that are stiff and lightweight at the same time, but they also have an increased functionality. For example, the load bearing mounting bracket of the star tracker could be redesigned with a cellular structure that mitigates shock loads. These structures were not implemented in the presented design, because no tools were available to support their design and analysis. Instead, the common and easily accessible topology optimization approach was utilized. Nevertheless, the presented redesign is superior to the original part, because fewer steps are necessary during the assembly and part weight is reduced significantly.

Acknowledgements

The authors acknowledge the support of this project by the Bayerische Hochschulzentrum für Lateinamerika (BAYLAT). Furthermore, we want to thank Matthias Killian and Katja Janzer from the Institute of Astronautics for supporting us with their expertise in thermal modelling.

Appendix A (Figures)

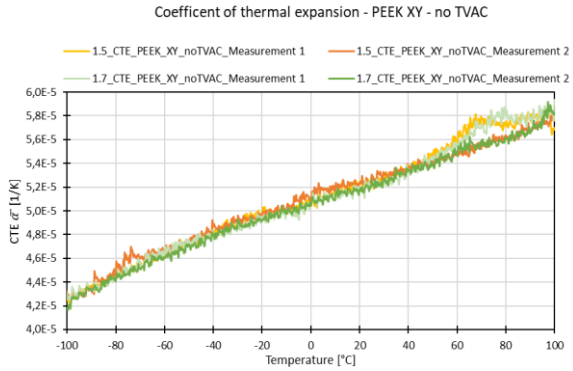

Fig. A1. Filtered CTE over temperature for XY printed PEEK before TVAC

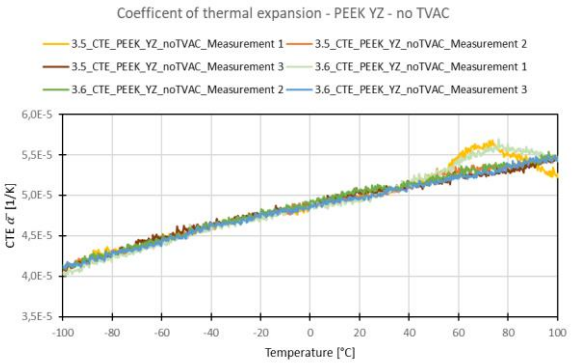

Fig. A2. Filtered CTE over temperature for YZ printed PEEK before TVAC

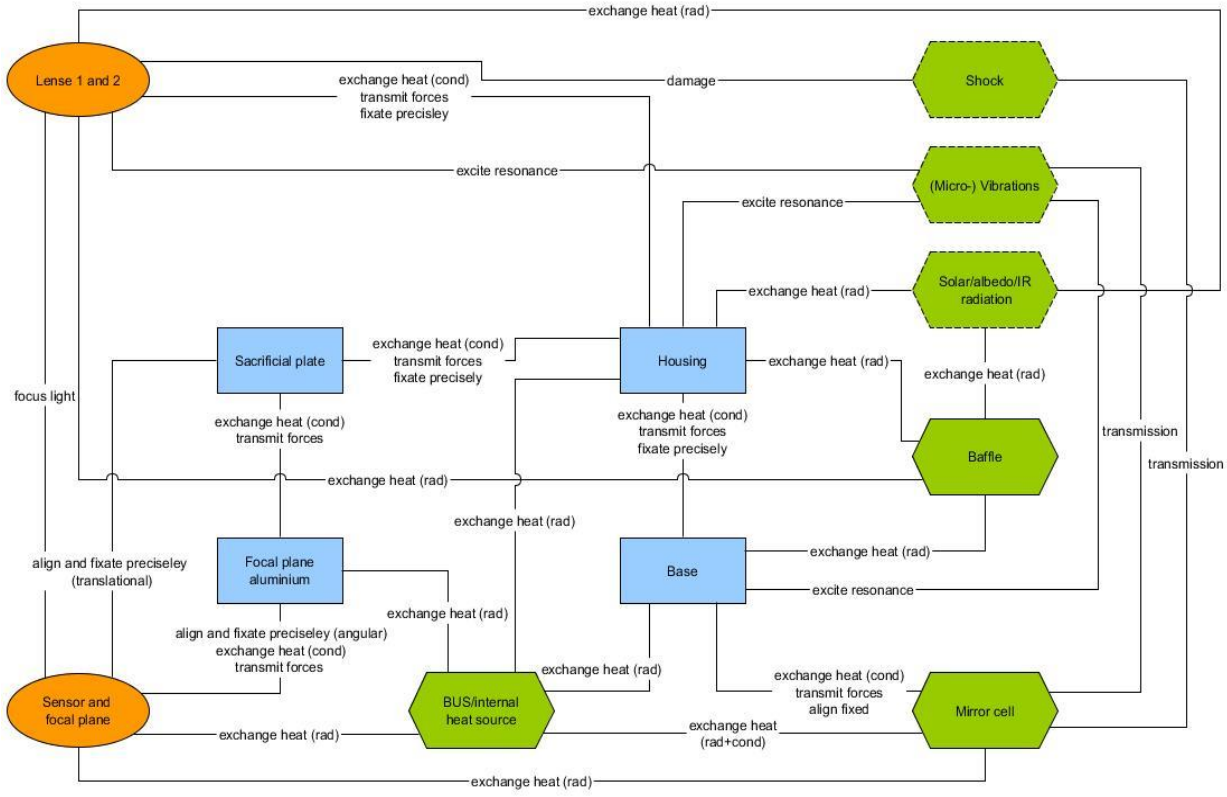

Fig. A3. Functional model of the star tracker

Appendix B (Tables)

Table B1. Morphological box containing various solutions for each subfunction

Subfunction	Solution 1	Solution 2	Solution 3	Solution 4
Maintain dimensional stability (thermo-structural)	Integrated insulation	Phase change material	Low thermal expansion material	Low/ zero thermal expansion lattice
Maintain dimensional stability (structural)	Nature-inspired structures	Turtle-inspired vault structuring	Topology optimization	
Enable adjustment of sensor	Compliant mechanism	Traditional approach		
Dissipate heat from sensor	Integrated thermal link	Integrated heat pipe	Increased radiator surface	Compliant mechanism louver
Mitigate shock loads	Particle damper	Auxetic lattice structures	Woodpecker-inspired shock absorber	

Table B2. Maximal temperature gradient within relevant parts and fluctuation of the average temperature within one orbit (detailed thermal model)

Case	Part	Maximal temperature gradient [°C]	Fluctuation of average temperature [°C]
Nominal case	Barrel	1,0	0,1
	Lens 1	0,8	0,1
	Lens 2	0,1	0,1
Cold case	Barrel	1,5	0,1
	Lens 1	0,8	0,1
	Lens 2	0,1	0,1
Hot case A*	Barrel	0,9	1,4
	Lens 1	1,1	1,2
	Lens 2	0,5	1,6
Hot case B*	Barrel	1,0	0,6
	Lens 1	0,8	0,5
	Lens 2	0,2	0,6

*event orbit only

Table B3. Maximal von Mises stress within barrel during nominal case

Load case	Time step [s]	Maximal von Mises stress [MPa]
1	0	66,7
2	600	66,6
3	1200	66,7
4	1800	66,8
5	2400	67,0
6	3000	67,2
7	3600	67,4
8	4200	67,4
9	4800	67,1
10	5400	66,9

Table B4. Maximal von Mises stress within barrel during hot case A

Load case	Time step [s]	Maximal von Mises stress [MPa]
1	6600	44,4
2	11597	65,6
3	17400	71,6
4	23400	73,2
5	29400	73,6
6	35220	73,6
7	41100	73,6
8	46920	73,5
9	52740	73,5
10	64380	73,4

References

[1] EOS, *EOS Titanium Ti64.* [Online] Available: https://cdn0.scrvt.com/eos/30716002f4859905/0cf7a9a6e4c3/EOS_Titanium_Ti64_de.pdf. Accessed on: 2017, Nov. 13.

[2] *Bestimmung der thermischen Längenänderung fester Körper - Teil 1: Grundlagen*, DIN 51045-1:2005-08, 2015.

[3] *Prüfung metallischer Werkstoffe - Zugproben*, DIN 50125, 2016.

[4] *Kunststoffe – Bestimmung der Zugeigenschaften – Teil 2: Prüfbedingungen für Form- und Extrusionsmassen*, DIN EN ISO 527-2, 2012.

[5] C. Gutierrez *et al.*, "CubeSat Fabrication through Additive Manufacturing and Micro-Dispensing," *44th International Symposium on Microelectronics 2011*, *IMAPS 2011*, http://www.cosmiacpubs.org/pubs/IMAPS2011_CassieGutierrezUTEP.pdf, 2011.

[6] *Thermal vacuum outgassing test for the screening of space materials*, ECSS-Q-ST-70-02C, 2008.

[7] Aerospace & Advanced Composites GmbH, *Standard Outgassing Test: ESA-certified according ECSS-Q-ST-70-02.* [Online] Available: http://www.aac-research.at/wp-content/uploads/2015/06/AAC_Standard_Outgassing_V01.pdf. Accessed on: 2017, Nov. 14.

[8] C. Klahn, B. Leutenecker, and M. Meboldt, "Design for Additive Manufacturing – Supporting the Substitution of Components in Series Products," *Procedia CIRP*, vol. 21, pp. 138–143, 2014.

[9] L. Stacheder, "TRIZ-based Biomimetic Part-Design for Additive Manufacturing," Master Thesis, iwb, Technische Universität München, München, 2015.

[10] C. Lindemann, T. Reiher, U. Jahnke, and R. Koch, "Towards a sustainable and economic selection of part candidates for additive manufacturing," *Rapid*

Prototyping Journal, vol. 21, no. 2, pp. 216–227, 2015.

[11] T. Kamps, M. Gralow, G. Schlick, and G. Reinhart, "Systematic Biomimetic Part Design for Additive Manufacturing," *Procedia CIRP*, vol. 65, pp. 259–266, 2017.

[12] J. Enright, D. Sinclair, and T. Dzamba, "The Things You Can't Ignore: Evolving a Sub-Arcsecond Star Tracker," *AIAA/USU Conference on Small Satellites*, https://digitalcommons.usu.edu/smallsat/2012/all2012/79, 2012.

[13] P. Yoder and D. Vukobratovich, *Opto-Mechanical Systems Design, Fourth Edition, Volume 1: Design and Analysis of Opto-Mechanical Assemblies*, 4th ed. Boca Raton, FL: CRC Press, 2015.

[14] C. Weyandt, "GN&C Lessons Learned from Multiple Missions," *AIAA/USU Conference on Small Satellites*, 2016.

[15] Daniel Vogel, "Combining Additive Manufacturing and Biomimicry for the Optimization of Satellite Structures," Master's Thesis, TUM, 2018.

[16] R. M. Fowler, L. L. Howell, and S. P. Magleby, "Compliant space mechanisms: A new frontier for compliant mechanisms," *Mech. Sci.*, vol. 2, no. 2, pp. 205–215, 2011.

[17] E. G. Merriam, J. E. Jones, and L. L. Howell, "Design of 3D-printed titanium compliant mechanisms," in *The 42nd Aerospace Mechanism Symposium*, Baltimore, MD, 2014.

[18] S. Simonian, V. Camelo, S. Brennan, N. Abbruzzese, and B. Gualta, "Particle Damping Applications for Shock and Acoustic Environment Attenuation," *49th AIAA/ASME/ASCE/AHS/ASC Structures, Structural Dynamics, and Materials Conference*, 2008.

[19] N. van Kevelaer, "Development of a Particle Damping Solution for PC-Boards in CubeSats," Master Thesis, Naval Postgraduate School, Monterey, California, 2016.

[20] T. Caffrey, T. Wohlers, and I. Campbell, *Wohlers Report: Annual Worldwide Progress Report*. Fort Collins: Wohlers Associates Inc., 2016.

[21] C. Dordlofva, A. Lindwall, and P. Törlind, "Opportunities and Challenges for Additive Manufacturing in Space Applications," in *NordDesign*, Trondheim, Norway, 2016.

[22] D. G. Gilmore, Ed., *Spacecraft Thermal Control Handbook: Volume I: Fundamental Technologies*, 2nd ed. El Segundo, California: The Aerospace Press, 2002.

[23] M. Fabbri and M. Molina, "IRIDIUM-NEXT Star Tracker Thermal Design: lessons learned and learning curve in a small series production," in *44th International Conference on Environmental Systems*, Tucson, Arizona, 2014.